

## A CFD STUDY OF PARTICLE FLOWS (PM1, PM10, PM100) IN LOW-VOLUME IMPACT SEPARATOR

Pannita Phiommark<sup>1</sup>, Chakrit Suvanjumrat<sup>1</sup>, Watcharapong Chookaew<sup>1</sup>, Sakchai Uaipipatanakul<sup>2</sup>, and  
\*Machimontorn Promtong<sup>1</sup>

<sup>1</sup>Department of Mechanical Engineering, Faculty of Engineering, Mahidol University,  
Salaya, Nakhon Pathom, 73170, Thailand

<sup>2</sup>Kinetics Corporation Ltd., 388 Ratchadapisek Rd.32 Chandrakasem,  
Chatuchak Bangkok 10900, Thailand

\*Corresponding Author, Received: 30 Nov. 2021, Revised: 21 Dec. 2021, Accepted: 30 Jan. 2022

**ABSTRACT:** Concerns around PM2.5 mean that discovering the number of soot particles and their size in ambient air is essential for general public health, so this research studies small particle flow behavior when separated by a low-volume impact separator. A Computational Fluid Dynamics (CFD) methodology was introduced to analyze the particle flow, and a simulation, where the actual operating flow rates and considered particle sizes were adopted as the initial conditions and material properties was performed. The flow pattern and particle's path inside the separator were numerically observed, and the performance in terms of the residence time and the trapped percentage was mainly discussed. The simulation results show that air velocity influenced particle traces and their distribution in the separator PM10 head, significantly smaller (PM1 and PM10). The residence time and the number of separated particles were used to evaluate the performance. Regarding the simulation results, after 5 seconds, the percentages of PM1, PM10, and PM100 could be escaped out of the PM2.5 Size Sorting Point about 44.2%, 37.6%, and 0%, respectively. In future work, a validation study will be performed, and the effects of internal structures that could affect the separator's performance will be investigated further. In addition, particle aggregations caused by flow vorticities that could cause dispersions will mainly be elucidated.

*Keywords: Particle Flow Simulation, Computational Fluid Dynamics (CFD), Discrete Phase Modelling (DPM), Performance Evaluation, Impact Separation Technique*

### 1. INTRODUCTION

Due to public health concerns, monitoring potentially harmful particulates (PM1, PM2.5, PM10) suspended in the air has become a pressing issue. Practically, the sizing and recognition of ingredients in the particles is a necessary task that provides information regarding the source of the particles, with the burning of crops, construction, and vehicles all widely named suspects. In certain circumstances, namely inside a building, particles can become virus carriers, which is relevant due to the COVID-19 pandemic. Therefore, the particulates could increase the spread of infected particles, leading to increased viral infection, directly affecting the population's health [1, 2]. Particle collectors/separators collect harmful particles and report real-time information [3, 4], but to accurately classify and calculate the particle size, investigation into the performance of particulate separators is required [5-9].

Recently, many researchers have developed techniques (i.e., cyclonic and impact methods) for the particle separators to classify ultrafine particle sizes [6, 8]. Peng [8] studied the efficiency of a cyclone to isolate PM2.5 by establishing a novel static chamber system. The polydisperse aerosol evaluated the performance of separators, testing the critical

parameters of the system. It also compared the separation efficiency curves of three cyclonic separators (VSCC-A, SCC-A, and SCC112). The results showed that VSCC-A had the most efficiency (with a slightly sharper cutoff curve). Tongling Xia and Chun Chen [10] studied the evolution of incense particles on nanofiber filter media. The results show that the removal efficiency for PM2.5 of nanofiber filter media decreased with the incense particle loading mass. The liquid aerosols were found to interact with the nanofiber network and enlarged the pore sizes. As found, when the loading mass was sufficiently large, the PM2.5 removal efficiency was constant.

Moreover, Zhanpeng Sun [3] studied a static cyclonic classifier and observed the flow characteristics. It was found that the primary flow was characterized by an upper vortex and a lower reverse vortex. The primary and secondary air occupied separate areas. Regardless of the inlet air velocity, the upward vortex represented a high flushing effect, reducing the retention of fine particles caused by higher-size particles. Prashant Patel [11] investigated a PM2.5 High-Volume Impactor (HVI) with a new inlet design. Also, the optimized D50 cutoff size of 2.52 $\mu$ m was investigated experimentally under the ambient conditions. The performance of the new

PM2.5 HVI sampler was investigated under various mass loading conditions, and it was shown to give comparable performance to commercial PM2.5 high- and low-volume samplers.

As known, Computation Fluid Dynamics (CFD) is widely used to investigate complex flows, which can be used to redesign thermal systems [12-16], which may represent particle flow circulations [17-23]. Kaltenbach and Laurien [18] studied the diffusion of radioactive particles inside a reactor building. A cycle simulating a catastrophic accident was analyzed using the CFD technique, where different droplets and particle size groups were introduced in this three-dimensional modeling. Ahmed [24] studied the Venturi Scrubber, an essential element of the Filtered and Closed Ventilation System (FCVS), which removes aerosols from polluted air. As mentioned, a CFD program named ANSYS CFX was used in the simulation to investigate the removal efficiency of Venturi Scrubbers operating in self-priming mode. Titanium oxide (TiO<sub>2</sub>) particles which were 1 micron in size, were used to replicate the powder particles. The removal efficiency was evaluated under the inlet air velocities of 1-3 m/s, and it was found that higher inlet air velocity led to more efficient removal of particles.

Similarly, Peng [25] proposed a hydraulic separator to remove pollutant particles and studied using the CFD technique. The ANSYS FLUENT program was used to simulate a hydrodynamic separator under complex initial conditions. As a result, the optimal angle between the overflow tube and the inlet tube for the removal of polluting particles was found. Fang [26] simulated a stone powder separator (SPS) using ANSYS FLUENT software, where a Discrete Phase Model (DPM) was introduced to simulate the crusher's airflow distribution and particle trajectory. The structure of the stone separation device and the suitable volume were optimized, and the simulation results were compared with experimental data. Therefore, the DPM is a promising model adopted in the CFD tool for the particle flow study.

## 2. RESEARCH SIGNIFICANCE

According to the complexity of the flow characteristics of particle matters, sometimes the CFD technique is utilized for elucidating the insight phenomenon. Specifically, this research will introduce the Discrete Phase Model (DPM) to observe particle flows inside the commercial impact separator. In particular, the observation will focus on how different particle sizes are distributed in the classifying chamber. In addition, the collector's performance in classifying the particles that are smaller than 10 microns (PM10) will be discussed.

Overall, the objective of this research is to utilize the CFD technique;

i) to investigate the effect of internal configurations and the flow characteristics in a commercial impact particle separator,

ii) to capture the particle paths (PM1, PM10, and PM100) under actual operation conditions,

iii) to study the effect of particle sizes, internal configurations and to address critical factors related to particle separation performance.

Apart from the flow variables and the particle's paths, the residence time and the number of escaped particles will be compared to evaluate the collection performance of the impact separator, which could lead to more understanding of designs of separators and possible solutions that enhance current performance.

## 3. FLUID FLOW AND PARTICLE FLOW EQUATIONS

### 3.1 Continuity Equation

The continuity equation reflects that mass is conserved (as shown in Eq. (1)). The equation is developed by adding the rate at which mass flows in and out of the control volume, and sets the net in-flow as the rate of change of mass within it. Since the mass velocity is continuous, hence this partial differential equation is called the continuity equation. Sometimes the first term can be omitted when the fluid flow is constant.

$$\frac{\partial \rho}{\partial t} + \rho \frac{\partial(\bar{u}_i)}{\partial x_i} = 0 \quad (1)$$

### 3.2 Momentum Equation

The momentum transfers within a control volume are conserved, hence the momentum equation, as shown in Eq. 2.

$$\frac{\partial \bar{u}_i}{\partial t} + \rho \bar{u}_j \frac{\partial \bar{u}_i}{\partial x_j} = - \frac{\partial \bar{p}}{\partial x_i} + \frac{\partial}{\partial x_j} \left[ \mu \left( \frac{\partial \bar{u}_i}{\partial x_j} + \frac{\partial \bar{u}_j}{\partial x_i} \right) - \rho \overline{u'_i u'_j} \right] \quad (2)$$

where

$$\tau_{ij} = -\rho \overline{u'_i u'_j} = \mu_t \left( \frac{\partial \bar{u}_i}{\partial x_j} + \frac{\partial \bar{u}_j}{\partial x_i} \right) - \frac{2}{3} \delta_{ij} \rho k \quad (3)$$

In Eqs. (1) - (2),  $\rho$  is a fluid density and  $\bar{p}$  is the system pressure. Here  $\bar{u}_i, \bar{u}_j$  are the average velocity components and  $\overline{u'_i u'_j}$  is the velocity fluctuation. The  $x_i, x_j$  terms are the coordinate axis. Equation (3) shows the Reynolds-Stress term ( $-\rho \overline{u'_i u'_j}$ )

### 3.3 Turbulence Model

The turbulence model is usually involved in calculating the continuity equations and the Reynolds-Averaged Navier-Stokes equations (RANS) in turbulent flow as the closure of the Reynolds Stress term. In general, an effective turbulence model must accurately calculate various flow behaviors, and the most popular turbulence model for turbulence simulation is the Launder and Spalding model (Eq. (4)), which is known as the Standard  $k-\varepsilon$  model. [27].

Later, the Standard  $k-\varepsilon$  turbulence model was modified to account for the difmodifit scales of the flow motions. Among the modifid versions of the  $k-\varepsilon$  model, the RNG  $k-\varepsilon$  (Re-Normalization Group k-epsilon) [28] was also popular to introduce to calculate the viscosity term for the gas-particle flow (see, Eq. (5) and Eq. (6)).

$$\mu_t = \rho C_\mu \frac{k^2}{\varepsilon} \quad (4)$$

where  $k$  is the kinetic energy of turbulence,  $\varepsilon$  is the rate of reduction in kinetic energy of turbulence,  $G_k$  is the production term of turbulence kinetic energy.

$k$  Equation:

$$\frac{\partial}{\partial x_i}(\rho k u_i) + \frac{\partial}{\partial t}(\rho k) = \frac{\partial}{\partial x_j} \left[ \left( \mu + \frac{\mu_t}{\sigma_k} \right) \frac{\partial k}{\partial x_j} \right] + P_k - \rho \varepsilon \quad (5)$$

$\varepsilon$  Equation:

$$\frac{\partial}{\partial x_i}(\rho \varepsilon u_i) + \frac{\partial}{\partial t}(\rho \varepsilon) = \frac{\partial}{\partial x_j} \left[ \left( \mu + \frac{\mu_t}{\sigma_\varepsilon} \right) \frac{\partial \varepsilon}{\partial x_j} \right] + C_{1\varepsilon} \frac{\varepsilon}{k} P_k - C_{2\varepsilon} \rho \frac{\varepsilon^2}{k} \quad (6)$$

where

$$C_{2\varepsilon}^* = C_{2\varepsilon} + \frac{C_\mu \eta^3 (1 - \eta/\eta_0)}{1 + \beta \eta^3}$$

and

$$\eta = S k / \varepsilon \quad S = (2S_{ij}S_{ij})^{1/2}$$

The model constants are

$$C_\mu = 0.0845, C_{1\varepsilon} = 1.42, C_{2\varepsilon} = 1.68, \eta_0 = 4.38, \sigma_k = 0.7194, \sigma_\varepsilon = 0.7194, \beta = 0.0012$$

The last term in equation (6),  $\rho \varepsilon$  represents the destruction rate, and  $P$  is the shear production buoyancy production term, given by:

$$P = \mu_t \frac{\partial u_i}{\partial x_j} \left( \frac{\partial \bar{u}_i}{\partial x_j} + \frac{\partial \bar{u}_j}{\partial x_i} \right) \quad (7)$$

### 3.4 Flow Equation of the Particles Phase

The particle motion equation is obtained by integrating the equilibrium force acting on the particle which is in the Lagrangian Frame [29]. While the particles move, they have resisted the velocity by drag and gravitational force. The terms of the force acting on the particle can be written as

$$\frac{du_p}{dt} = F_D(\mathbf{u} - \mathbf{u}_p) + \frac{g_x(-\rho)}{\rho_p} + F_x \quad (8)$$

where  $\mathbf{u}$  is the fluid phase velocity and  $\mathbf{u}_p$  is the particle velocity. The term  $\mu$  is the molecular viscosity of the fluid. Also,  $\rho$  is the fluid density and  $\rho_p$  is the density of the particles. For the forms,  $F_x$  and  $F_D$  are an additional acceleration and drag force per unit particles mass, respectively.

$$F_D = \frac{18\mu c_D Re}{\rho_p d_p^2 24} \quad (9)$$

$Re$  is the relative Reynolds number is given by

$$Re = \left( \frac{\rho d_p (u_p - u)}{\mu} \right) \quad (10)$$

where  $d_p$  is the particle's diameter.

## 4. RESEARCH METHODOLOGY

The research methodology is illustrated in Fig. 1, and the main task was to perform a simulation of the particle flows in the particle separator. Before using the CFD method to simulate the particle flow, the steady-state flow's initial stage is required (running the case without the particles). Afterward, the considered particle sizes were adopted into the simulation, and the flows are monitored.

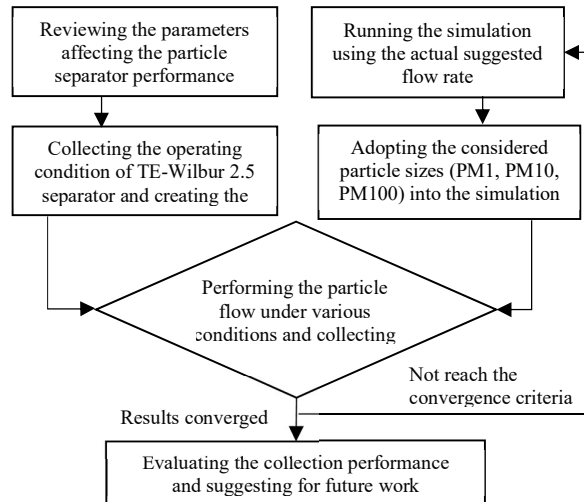


Fig. 1 The flow chart representing the research methodology

The results, including the velocity patterns for each particle size and the residence time were discussed regarding the separation capability. By adopting different operating conditions, hopefully, the ideas for further development and designs could be established.

#### 4.1 Details of the Particle Separator

There are two available functions of the TE-Wilbur 2.5 particle separator (Fig. 2a). The first is to collect dust-sized lower than PM10 microns, and this function utilizes an impact technique to separate the particle size. It can be seen in Figure 2b after the particles hit a solid plate, the larger particle (PM10 above) may be trapped and the smaller may be flown through to another function at the screening tube (PM10 dust screening unit). For the second mode, the separation of dust particles that are equal to or smaller than PM2.5 is separated using a cyclonical separator, which sends particle sizes smaller than PM2.5 into the sampling room and larger sizes to another collector.

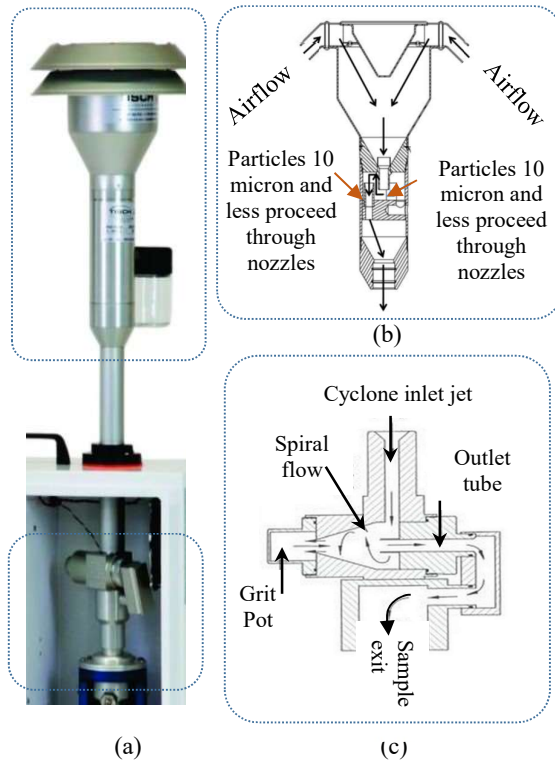


Fig. 2 PM10 and PM2.5 particle size sorting head (a) with internal structure details, PM10 size sorting point (b), and PM2.5 size sorting point (c)

#### 4.2 Meshing

The 3D model of the separation head after the meshing process is shown in Fig. 2. It should be noted that a mesh independence study was conducted to

observe the influence of the element number. The velocity at the center of the chamber was chosen to compare among different mesh cases for finding the suitable mesh in terms of giving both accuracy and efficiency while running the simulations.

As a result (Figure 3), the velocity was not significantly changed when the mesh element was used at about 150,000 [23]. Therefore, this number of mesh sizes was adopted for further numerical investigation. In this simulation study, 16.67 L/min (0.0675 m/s) of the volumetric flow rate was adopted for the velocity inlet and this number is suggested by the manufacturer for the real operation.

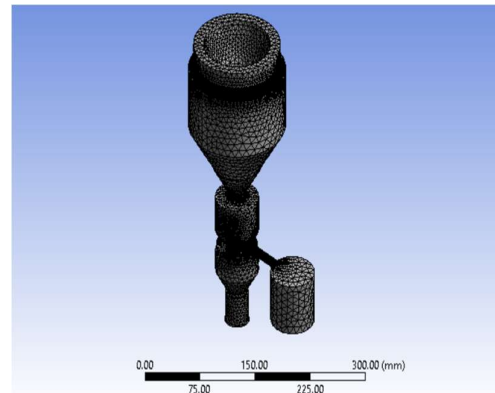


Fig. 3 The 3D separation head (PM10) after the meshing process

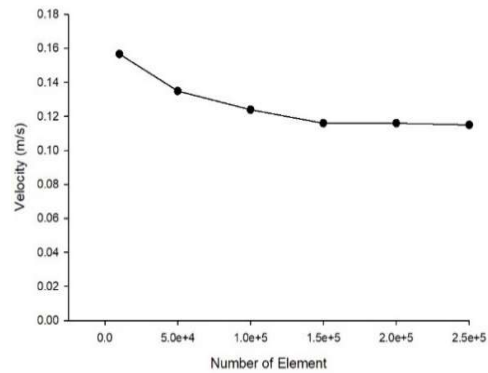


Fig. 4 Total mesh used for the separator model (the mesh independence study)

## 5. RESULTS AND DISCUSSIONS

In this section, the simulation results of the particle separator will be presented and discussed. Firstly, the velocity profiles in the separator system will be given, and it discusses the flow paths of different particle sizes (PM1, PM10, and PM100). Lastly, the number of escaped particles will be discussed to evaluate the collection performance. It should be noted that only the PM10 separator system

was investigated and evaluated in terms of the impact technique and sizing performance.

### 5.1 The Velocity Pattern

Usually, local flow velocity reflects a particle's path in the separator, so observing the flow pattern in the primary chamber is necessary. The velocity streamlines of the PM10 particles in the separator system are shown in Fig.5. It is seen that the vortexes occurred at the top of the primary chamber (see in Fig. 5a and Fig. 5b). This may be because of having high velocity at the inlet and the lower velocities near the primary chamber surface (Fig. 5b), so the difference in velocities and the internal configuration could lead to a presence of the circulations [30]. It should be noted that without a suitably designed cone inside the separator head, the air circulations would have not happened [31].

As can be seen in Figure 5a, the maximum velocity found at the connecting tube linking the separation chamber was 4.30 m/s. Fig. 5c presents the flow velocity where the inlet velocity was halved. On average, the velocities in the primary chamber were reduced to be halved. When there is a smaller gap between the inlet velocity and the near-wall velocity, smaller vortexes were found near the top of the chamber. Moreover, the maximum velocity in the connecting tube also decreased.

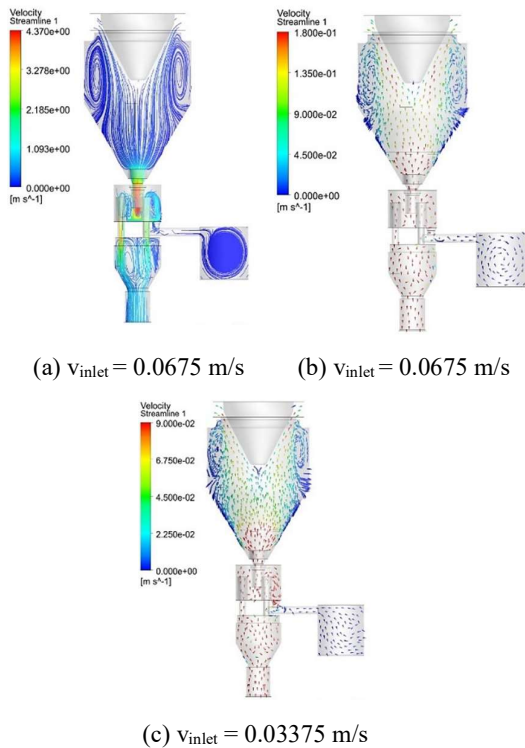


Fig. 5 Velocity streamlines and vectors occurring inside the separator system

Figure 6 compares the flow patterns in the separation chamber when air only flows through half of the velocity inlet. As shown, when the airflow in the chamber impacts the bottom and flows to the walls, circulations are caused inside the collecting room. As it is a small chamber recognition of differences in the flow circulation in the separation room is difficult.

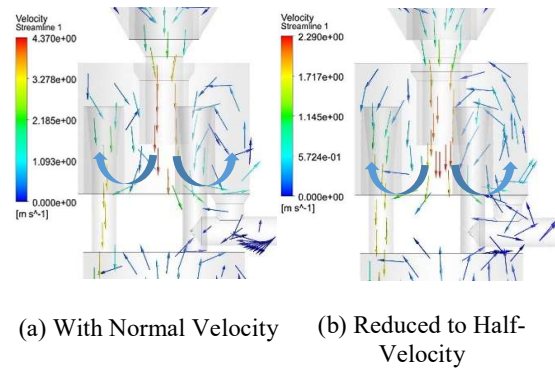


Fig. 6 Velocity streamlines in the separation chamber

### 5.2 The Paths of Particles

In this section, the paths of the differently sized particles are presented under the same operating conditions. Fig.7a shows the paths of 1  $\mu$ m and 10  $\mu$ m sized particles, and Fig. 7b shows the paths of 1  $\mu$ m and 100  $\mu$ m sized particles. In both cases, the particles were tracked from the inlet and the final time captured was at 5 seconds.

When the particles were injected, the large dust particles (10 $\mu$ m and 100 $\mu$ m) fell into the middle of the primary chamber due to the dominant inlet velocity. However, the 1 $\mu$ m micron particles swirled near the top longer than the 10 $\mu$ m and 100 $\mu$ m particles, which could be because they were pushed away from the regions with heavy turbulence.

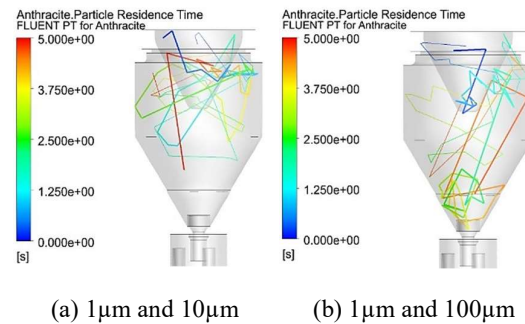


Fig. 7 The path of interested particle sizes

Figures 8a and Fig. 8b present the path of the dust particles sized at 1 $\mu$ m and 100 $\mu$ m. It should be noted

that the case of fig. 8b, the pipe length was half of the original height. The residence time (shown on both figures), confirms that the smaller particles take longer to leave the separation chamber in the case the tube long was halved, which could be the result of the height of the unsuitable collecting area or the tube to collect the smaller particles.

In the case of 100µm particles, although the particles could enter the separation chamber, however, within the consideration time (45s), the particles were still trapped in the separation unit. This can confirm that the size bigger than 10µm cannot be escaped out of the PM10 size sorting chamber [32].

More details regarding the time required to enter the separation chamber and the time required to escape from the separator are given in Table 1. Interestingly, it shows that the escape time required for the smaller particles with the original tube length was less than with the half-long tube. More evidence is required to conclude the influence of the collecting tube length.

Table 1 Comparisons for the separation of 1µm and 100µm particles

Case Study	Particle Size	Time of Entry into Separation Chamber	Time of Escape
Normal	1 µm	19.2s	25.1s
Long	100 µm	4.9s	-
Half-Long	1 µm	39.2s	45.4s
Long	100 µm	2.9s	-

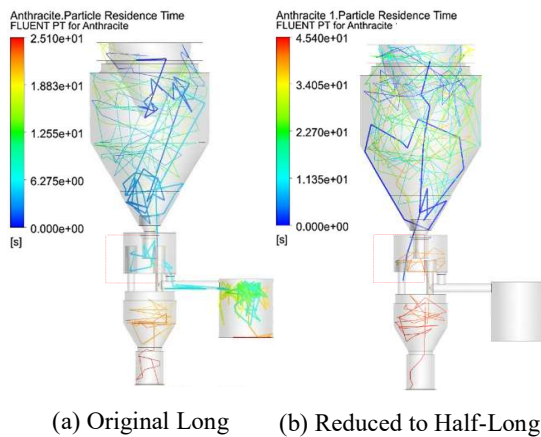


Fig. 8 The path of particles 1µm and 100µm in size when the collecting tube

### 5.3 The Collection Performance

In Fig. 9-11, the Particle Residence Times (PRT) of each particle size (1µm, 10µm, and 100µm) are presented. It should be noted that the end time for this

tracking was 5 seconds, so it is possible to have small changes in terms of the number of escaped and remaining particles inside the separator.

Clearly, after 5 seconds, the large particles (100µm) were unable to be separated, which is relevant to the design objective that this system should allow only the particle sizes equal and/or smaller than 10 µm flow through. This could be because the flow constantly pushed the particle flow towards the floor of the separation chamber.

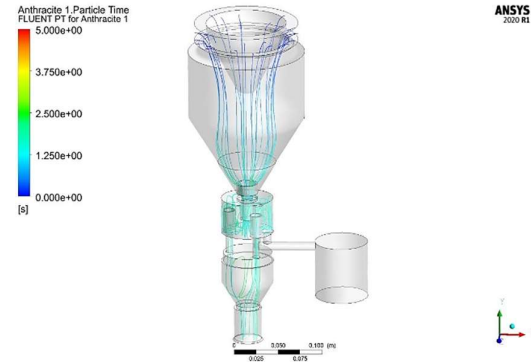


Fig. 9 Particle residence time (PRT) of 1µm sized particles

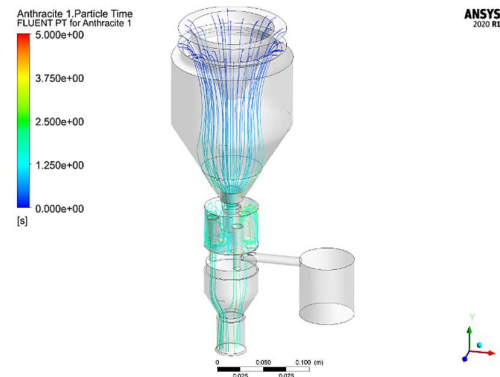


Fig. 10 Particle residence time (PRT) of 10µm sized particles

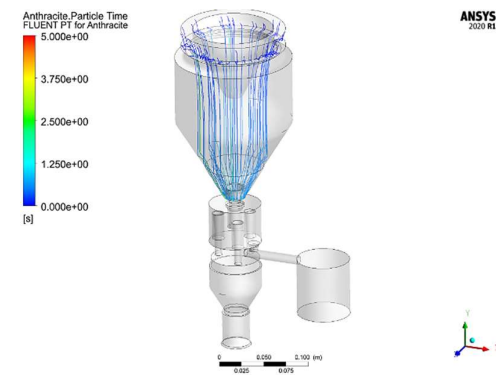


Fig. 11 Particle residence time (PRT) of 100µm sized particles

Table 2 The Calculated Collection Performance when the Tracking Time Ended at 5 Seconds

Size (µm)	No. of (#) the Particles Injected	# Remaining	# Escaped	Escaped Percent
1	708	395	313	44.2%
10	706	440	266	37.6%
100	706	706	0	0%

As shown in Table 2, 44% and 37% of the 1µm and 10µm are the percents of the particles separated from the PM2.5 size sorting point within 5 seconds. Nevertheless, the number of the escaped particles at sizes 1µm and 10µm could increase if the observation time was expanded.

## 6. CONCLUSION AND FUTURE WORK

The simulation of the particle flow in the TE-Wilbur 2.5 particle separator impact system has been performed. It was found that the particles sized at 10 microns (PM10) or less can be separated by the collector, but not for particles sized at 100 microns (PM100). The introduction of the Computational Fluid Dynamics (CFD) technique allows the separation performance and the path of particles to be investigated. Overall, the conclusions that can be drawn are as follows:

i) The secondary flow (vortexes) occurred near the top of the primary chamber. These flow circulations could be the result of the high inlet velocity and the internal geometry of the impact system. The average velocity inside the primary chamber was less than 0.5 m/s; however, the velocity inside the connecting tube before entering the impacting room was as high as 4.37 m/s.

ii) By tracking the paths of PM1, PM10, and PM100 particles, it was found that smaller particles (PM1 and PM10) swirled inside the primary chamber longer than the larger particles (PM100).

iii) When reducing the length of the separating tube (to half the original length) it was found that the residence time of small particles was longer than when they entered from the original length tube. This may be because of the velocity profiles (circulation) in the separation chamber.

iv) At the end of the collection time (5 seconds), the collection performance of the impact stem for PM1, PM10, and PM100 sized particles were 44.2%, 37.6%, and 0%, respectively.

In future work, an experimental study will be conducted, and a validation study will be performed. Further investigations will optimize the operating conditions and internal structure of the impact and cyclonic systems of the particle separator.

## 7. ACKNOWLEDGMENTS

Many thanks to the Mechanical Engineering Department, Faculty of Engineering, Mahidol University, for allowing us to use the laboratory. Thanks to CADFEM SEA Pte. Ltd. - A certified Elite Channel Partner to ANSYS - for providing support and access to the CFD program named ANSYS Fluent 2021 R1.

Also, many thanks to Kinetics Corporation Ltd. and the National Research Council of Thailand (NRCT Project ID 960692) for financial support.

Especially, the authors would like to thank Robert McEvoy, from the Faculty of ICT at Mahidol University for editing and proofreading the manuscript.

## 8. REFERENCES

- [1] Vuorinen V., Aarnio M., Alava M., Alopaeus V., Atanasova N., Auvinen M., Balasubramanian N., Bordbar H., Erasto P., Grande R., Hayward N., Hellsten A., Hostikka S., Hokkanen J., Kaario O., Karvinen A., Kivisto I., Korhonen M., Kosonen R., Kuusela J., Lestinen S., Laurila E., Nieminen H.J., Peltonen P., Pokki J., Puisto A., Raback P., Salmenjoki H., Sironen T. and Osterberg M., Modelling aerosol transport and virus exposure with numerical simulations in relation to SARS-CoV-2 transmission by inhalation indoors. *Saf Sci*, 2020. 130: p. 104866.
- [2] W.H.O. Coronavirus disease (COVID-19): How is it transmitted? 2020 01/05/2021; Available from: <https://www.who.int/news-room/q-a-detail/coronavirus-disease-covid-19-how-is-it-transmitted>.
- [3] Sun Z., Sun G., Peng P., Liu Q. and Yu X., A new static cyclonic classifier: Flow characteristics, performance evaluation, and industrial applications. *Chemical Engineering Research and Design*, 2019. 145: p. 141-149.
- [4] Mui W., Mai H., Downard A.J., Seinfeld J.H. and Flagan R.C., Design, simulation, and characterization of a radial opposed migration ion and aerosol classifier (ROMIAC). *Aerosol Science and Technology*, 2017. 51(7): p. 801-823.
- [5] Prasanna N., Subramanian K., Ajay S., Rajagopal T. and Vigneshwaran V., CFD study on the performance of reducing pressure drop holes in a cyclone separator. *Materials Today: Proceedings*, 2021. 43: p. 1960-1968.
- [6] Lin W.-Y., Hsiao T.-C. and Hong B.-L., Improving the removal efficiency of fine particulate matters in air pollution control devices: Design and performance of an electrostatic aerosol particle agglomerator.

- Journal of the Taiwan Institute of Chemical Engineers, 2020. 107: p. 110-118.
- [7] Zhang H. and Liu Q., Numerical investigation on the performance of moisture separator: Experimental validation, applications, and new findings. *Annals of Nuclear Energy*, 2020. 142.
- [8] Du P., Liu J., Gui H., Zhang J., Yu T., Wang J., Cheng Y., Lu Y., Yao Y., Fu Q. and Chen C., Development of a static test apparatus for evaluating the performance of three PM2.5 separators commonly used in China. *J Environ Sci (China)*, 2020. 87: p. 238-249.
- [9] Wang S., Li H., Wang R., Wang X., Tian R. and Sun Q., Effect of the inlet angle on the performance of a cyclone separator using CFD-DEM. *Advanced Powder Technology*, 2019. 30(2): p. 227-239.
- [10] Xia T. and Chen C., Toward understanding the evolution of incense particles on nanofiber filter media: Its influence on PM2.5 removal efficiency and pressure drop. *Building and Environment*, 2020. 172.
- [11] Patel P., Aggarwal S.G., Tsai C.-J. and Okuda T., Theoretical and field evaluation of a PM2.5 high-volume impactor inlet design. *Atmospheric Environment*, 2021. 244.
- [12] Promtong M., Khunsri K., Teachapanitvittaya K., Trakulkumrue T., Watechagit S. and Suvanjumrat C., Experimental and Numerical Investigations into the Natural Convection of Hot Gas in a Vertical Smoking Oven: A Validation Study, in *The 34th Conference of the Mechanical Engineering Network of Thailand*. 2020: 15 - 17 July 2020, Prachuap Khiri Khan, Thailand.
- [13] Tekasakul P. and Promtong M., Energy efficiency enhancement of natural rubber smoking process by flow improvement using a CFD technique. *Applied Energy*, 2008. 85(9): p. 878-895.
- [14] Promtong M. and Tekasakul P., CFD study of flow in natural rubber smoking-room: I. Validation with the present smoking room. *Applied Thermal Engineering*, 2007. 27(11-12): p. 2113-2121.
- [15] Promtong M., CFD study of flow in rubber smoking room and modification to improve the uniformity of velocity and temperature distributions. 2006, Prince of Songkla University.
- [16] Promtong M., Kirirat P., Taweekun J. and Tekasakul P., CFD, and Experimental Study of the Temperature Distribution in a Present Rubber Smoking Room, in *The 19th Conference of Mechanical Engineering Network of Thailand*. 2005: 19-21 October 2005, Phuket, Thailand.
- [17] Ren J., Wang Y., Liu Q. and Liu Y., Numerical Study of Three Ventilation Strategies in a prefabricated COVID-19 inpatient ward. *Build Environ*, 2021. 188: p. 107467.
- [18] Kaltenbach C. and Laurien E., CFD Simulation of aerosol particle removal by water spray in the model containment THAI. *Journal of Aerosol Science*, 2018. 120: p. 62-81.
- [19] Xu G. and Wang J., CFD modeling of particle dispersion and deposition coupled with particle dynamical models in a ventilated room. *Atmospheric Environment*, 2017. 166: p. 300-314.
- [20] Brusca S., Famoso F., Lanzafame R., Mauro S., Messina M. and Strano S., PM10 Dispersion Modeling by Means of CFD 3D and Eulerian-Lagrangian Models: Analysis and Comparison with Experiments. *Energy Procedia*, 2016. 101: p. 329-336.
- [21] Sajjadi H., Tavakoli B., Ahmadi G., Dhaniyala S., Harner T. and Holsen T.M., Computational fluid dynamics (CFD) simulation of a newly designed passive particle sampler. *Environ Pollut*, 2016. 214: p. 410-418.
- [22] Dickenson J.A. and Sansalone J.J., Discrete phase model representation of particulate matter (PM) for simulating PM separation by hydrodynamic unit operations. *Environ Sci Technol*, 2009. 43(21): p. 8220-6.
- [23] Udaya Bhaskar K., Rama Murthy Y., Ramakrishnan N., Srivastava J.K., Sarkar S. and Kumar V., CFD validation for fly ash particle classification in hydro cyclones. *Minerals Engineering*, 2007. 20(3): p. 290-302.
- [24] Ahmed S., Mohsin H., Qureshi K., Shah A., Siddique W., Waheed K., Irfan N., Ahmad M. and Farooq A., Investigation of dust particle removal efficiency of self-priming venturi scrubber using computational fluid dynamics. *Nuclear Engineering and Technology*, 2018. 50(5): p. 665-672.
- [25] Peng Y., Zhang Z., Yao J.-J., Zhou Y., Cai S., Zhang J., Li Y., Kong Y. and Zhang W., Computation fluid dynamics model of first-flush runoff through a hydrodynamic separator. *Journal of Cleaner Production*, 2019. 241.
- [26] Fang H., Yang J., Song Y., Huang W. and Chen J., Simulation and experimental study on the stone powder separator of a vertical shaft impact crusher. *Advanced Powder Technology*, 2020. 31(3): p. 1013-1022.
- [27] Mothilal T. and Pitchandi K., Influence of inlet velocity of the air and solid particle feed rate on holdup mass and heat transfer characteristics in the cyclone heat exchanger. *Journal of Mechanical Science and Technology*, 2015. 29(10): p. 4509-4518.
- [28] Yakhot V., Orszag S.A., Thangam S., Gatski T.B. and Speziale C.G., Development of turbulence models for shear flows by a double

- expansion technique. *Physics of Fluids A: Fluid Dynamics*, 1992. 4(7): p. 1510-1520.
- [29] Yin S., Nie W., Guo L., Liu Q., Hua Y., Cai X., Cheng L., Yang B. and Zhou W., CFD simulations of air curtain dust removal effect by ventilation parameters during tunneling. *Advanced Powder Technology*, 2020. 31(6): p. 2456-2468.
- [30] Chen X., Yu J. and Zhang Y., The use of axial cyclone separator in the separation of wax from natural gas: A theoretical approach. *Energy Reports*, 2021. 7: p. 2615-2624.
- [31] Bnà S., Ponzini R., Cestari M., Cavazzoni C., Cottini C. and Benassi A., Investigation of particle dynamics and classification mechanism in a spiral jet mill through computational fluid dynamics and discrete element methods. *Powder Technology*, 2020. 364: p. 746-773.
- [32] Elsayed K. and Lacor C., Numerical modeling of the flow field and performance in cyclones of different cone-tip diameters. *Computers & Fluids*, 2011. 51(1): p. 48-59.

---

Copyright © Int. J. of GEOMATE All rights reserved,  
including making copies unless permission is obtained  
from the copyright proprietors.

---

**Filename:** 53-61-gxi310-Pannita-March-2022-91.docx  
**Directory:** C:\Users\Dell\Documents  
**Template:** C:\Users\Dell\AppData\Roaming\Microsoft\Templates\Normal.dotm  
**Title:** AUTHOR'S GUIDELINES  
**Subject:**  
**Author:** Sonny  
**Keywords:**  
**Comments:**  
**Creation Date:** 05/01/2022 13:43:00  
**Change Number:** 9  
**Last Saved On:** 02/02/2022 15:07:00  
**Last Saved By:** Dell  
**Total Editing Time:** 56 Minutes  
**Last Printed On:** 02/02/2022 15:07:00  
**As of Last Complete Printing**  
**Number of Pages:** 9  
**Number of Words:** 6,958 (approx.)  
**Number of Characters:** 39,663 (approx.)